Materials Science and Engineering C 49 (2015) 700–712

Contents lists available at ScienceDirect

Materials Science and Engineering C

journal homepage: www.elsevier.com/locate/msec

In vitro evaluation of alginate/halloysite nanotube composite scaffolds for tissue engineering

Mingxian Liu [a], Libing Dai [b], Huizhe Shi [c], Sheng Xiong [c], Changren Zhou [a,*]

[a] Department of Materials Science and Engineering, Jinan University, Guangzhou 510632, China
[b] Guangzhou Institute of Traumatic Surgery, Guangzhou Red Cross Hospital Medical College, Jinan University, Guangzhou 510220, China
[c] Institute of Biomedicine, National Engineering Research Center of Genetic Medicine, Jinan University, Guangzhou 510632, China

ARTICLE INFO

Article history:
Received 2 September 2014
Received in revised form 21 December 2014
Accepted 7 January 2015
Available online 9 January 2015

Keywords:
Alginate
Halloysite
Scaffold
Compressive property
Biocompatibility

ABSTRACT

In this study, a series of alginate/halloysite nanotube (HNTs) composite scaffolds were prepared by solution-mixing and freeze-drying method. HNTs are incorporated into alginate to improve both the mechanical and cell-attachment properties of the scaffolds. The interfacial interactions between alginate and HNTs were confirmed by the atomic force microscope (AFM), transmission electron microscope (TEM) and FTIR spectroscopy. The mechanical, morphological, and physico-chemical properties of the composite scaffolds were investigated. The composite scaffolds exhibit significant enhancement in compressive strength and compressive modulus compared with pure alginate scaffold both in dry and wet states. A well-interconnected porous structure with size in the range of 100–200 μm and over 96% porosity is found in the composite scaffolds. X-ray diffraction (XRD) result shows that HNTs are uniformly dispersed and partly oriented in the composite scaffolds. The incorporation of HNTs leads to increase in the scaffold density and decrease in the water swelling ratio of alginate. HNTs improve the stability of alginate scaffolds against enzymatic degradation in PBS solution. Thermogravimetrica analysis (TGA) shows that HNTs can improve the thermal stability of the alginate. The mouse fibroblast cells display better attachment to the alginate/HNT composite than those to the pure alginate, suggesting the good cytocompatibility of the composite scaffolds. Alginate/HNT composite scaffolds exhibit great potential for applications in tissue engineering.

1. Introduction

Alginate, a natural polysaccharide extracted from brown seaweeds, is a biocompatible polymer widely used in tissue engineering, cell therapy, and drug delivery [1–3]. As tissue engineering scaffold materials, it has many advantages such as highly hydrophilic, biodegradable, biocompatible, derived from biomass resources, easy to crosslink, and possessing high mechanical property [4–7]. Chemically, alginate is a linear polymeric acid composed of 1,4-linked β-D-mannuronic acid (M) and α-L-guluronic acid (G) residues. Alginate can form crosslink networks through ionic interactions between divalent cations (e.g., Ca^{2+}, Sr^{2+} and Ba^{2+}) and the carboxyl functional group of G units. Crosslinking makes alginate insoluble in aqueous solution and culture medium. This enables it to remain as supporting structure in the form of hydrogel for the seeded cells when it is used as a scaffold both in vitro and in vivo. When used in vivo, ionically crosslinked alginate degrades when the calcium ions are exchanged with other ions in the body, such as Na^{+}. So, after finishing the mission of supporting cell growth, alginate can be gently removed by the body circulation systems. Due to these characters, alginate has attracted many attentions in the development of polymeric delivery systems and tissue engineering scaffold [2,5,8]. The correct physical properties and cellular compatibility are the major factors that determine the suitability of alginate used as tissue engineering scaffold materials.

The composite scaffolds composed of nanoparticles and biopolymer, and with a well-defined porous microstructure, as biocompatible and biodegradable supports for cell growth have been developed in recent years. For instance, carbon nanotubes (CNTs) were incorporated into the alginate for improving the mechanical properties and the cell adhesion properties [7]. 1% (w/w) single-walled CNT increased the tensile strength of alginate struts from 436 to 542 kPa, and the tensile modulus was increased from 287.5 to 426 kPa [7]. CNTs also could effectively play the role of crosslinker in the alginate hydrogel, which led to a faster gelling time and a superior resistance to compressive deformation [9]. The alginate–CNTs gel showed mild tissue response but no adverse effect. Halloysite nanotubes (HNTs) are novel natural one-dimensional particles with a unique tubular microstructure and an aspect ratio of ~20. HNTs have wide applications in catalysis, ceramic, nano-reactor, cosmetic, and polymer nanofiller [10,11]. As reinforcement for polymers used in tissue engineering scaffold, the tubes have advantages over other nanoparticles such as hydrophilicity, good dispersion ability, biocompatibility, entrapment of drugs, and low cost. Our previous study showed that HNTs could improve the compression properties of

* Corresponding author.
E-mail address: tcrz9@jnu.edu.cn (C. Zhou).

http://dx.doi.org/10.1016/j.msec.2015.01.037
0928-4931/

chitosan scaffolds significantly, while the cell attachment and skin repairing property of the chitosan were also increased [12–14]. HNTs were also incorporated into alginate to form hydrogel beads for removing dyes and heavy metals in wastewater as well as for controlled-release of drugs [4,15–17]. Recently, the alginate/HNT nanocomposite hydrogels were developed for sustained releasing of bone morphogenetic proteins [18]. An improvement in mechanical strength of the alginate by HNTs has been attributed to the physical interactions (hydrogen bonds) between the alginate and HNTs.

To our best knowledge, no study has been reported on the preparation and the physicochemical properties of 3D porous alginate/HNT composite scaffolds. To better ascertain the application potential of this composite scaffolds in tissue engineering, this study aims at analyzing the key properties of alginate/HNT composite, i.e., (a) the interfacial interactions of HNTs with the alginate polymer, (b) the influence of HNTs on the physicochemical properties of alginate scaffolds, (c) the mechanical behavior of the composite scaffolds, and (d) the cell attachment behavior on the composite scaffolds. Due to the high mechanical properties, proper porous microstructure, and good cytocompatibility, the prepared porous alginate/HNT scaffolds have potential applications in tissue engineering.

2. Experimental

2.1. Materials

Sodium alginate with a medium range molecular weight was purchased from Sigma-Aldrich. Halloysite nanotubes (HNTs), mined from Hunan Province, China, were used after purification. Calcium chloride ($CaCl_2$) and other chemicals used in this study were of analytical grade and were used as received. Ultrapure water from RO-DI® Laboratory water purification system was used to prepare the aqueous solutions.

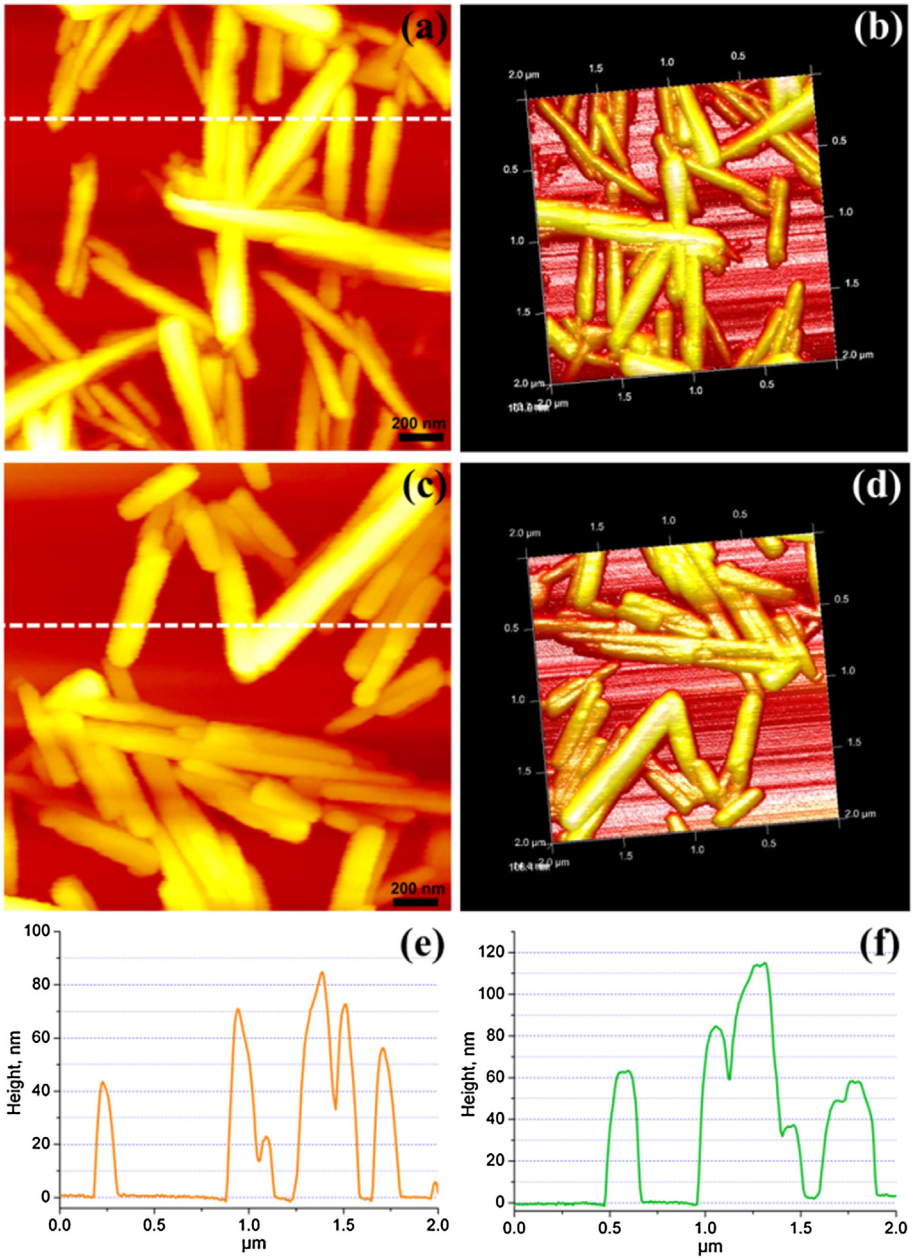

Fig. 1. AFM height ((a) and (c)) and 3D images ((b) and (d)), and the line scanning height profile ((e) and (f)) of HNTs (a, c, e) and alginate–HNTs (1:1) (b, d, f).

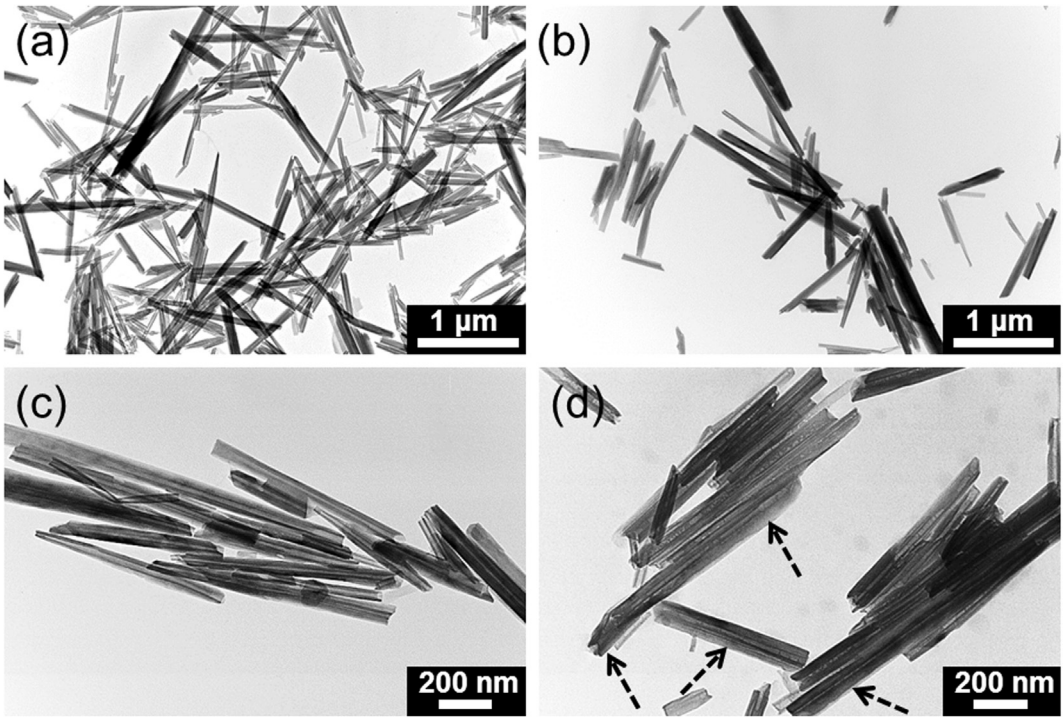

Fig. 2. TEM for HNTs ((a) and (c)) and alginate–HNTs (weight ratio, 2:1) ((b) and (d)). The black arrows represent the alginate layer around the tubes.

2.2. Fabrication of alginate/HNT composite scaffolds

Alginate/HNT composite scaffolds were prepared by solution-mixing and freeze-drying method. Typically, HNTs were dispersed in 100 mL of ultrapure water using a magnetic stirrer for 10 min. Subsequently, the dispersion was subjected to ultrasonic treatment in an ice bath for 30 min. 2 g of alginate powder was subsequently added to the dispersion. The mixture dispersion was continuously stirred overnight and then treated by ultrasonic for 1 h under 4 °C in order to obtain the good dispersion of the nanotubes. Then the solutions were poured into cylinder plastic mold with 10 mm in diameter and 10 mm in height. Afterward, they were frozen into ice at −20 °C overnight in a refrigerator and then lyophilized at −80 °C using a Christ freeze dryer ALPHA 1-2/LD plus. The scaffolds were immersed in 5% $CaCl_2$ solution overnight to crosslink the polymer chains and freeze-dried again. The sample codes of the composite scaffold (Al2N1, Al1N1, Al1N2, Al1N4) represented the weight ratio of alginate (Al) and HNTs (N). For example, in the Al2N1 composite scaffold the weight ratio of alginate and HNTs was 2:1. For comparison, pure alginate scaffold was also prepared in the same way but without addition of HNTs. All the samples were kept in a vacuum desiccator at room temperature before any measurements.

2.3. Characterization of the interactions between alginate and HNTs

To evaluate the surface morphology of pristine HNTs and alginate–HNTs, a multimode AFM with NanoScope IIIa controller was used (Veeco Instruments). The dilute HNTs aqueous dispersion and alginate–HNT (1:1, w/w) solution were dispersed on a piece of freshly cleaved mica and images were collected under contact mode using a soft cantilever (NP-S20, Veeco, force constant ca. 0.1 nN/nm). The dilute HNTs aqueous dispersion and alginate–HNT aqueous solutions were also dipped and dried on the carbon-film supported Cu-grid. Then the samples were observed using Philips Tecnai 10 TEM under accelerating voltage of 100 kV. Zeta potential of dilute HNTs and alginate–HNT (2:1, weight ratio) aqueous dispersion (0.05 wt.%) was measured using a Zetasizer Nano ZS (Malvern Ltd., UK).

2.4. Characterization of alginate/HNT composite scaffolds

2.4.1. Fourier transform infrared spectroscopy (FTIR)

The FTIR spectra of the dried scaffold samples were measured using attenuated total reflectance (ATR) model using VERTEX 70 (Bruker, USA). Thirty-two consecutive scans were taken and their average was stored. Spectra were taken from 4000 to 400 cm^{-1}. The resolution of the wavenumber was 2 cm^{-1}.

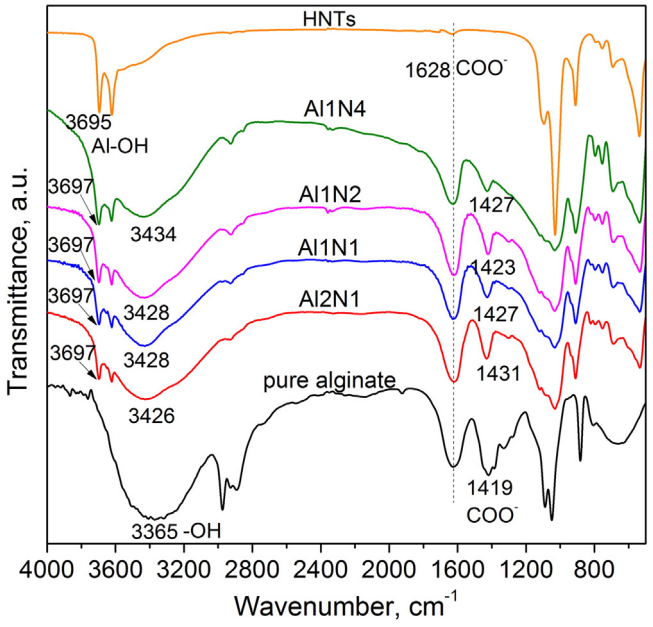

Fig. 3. FTIR of pristine HNTs, freeze-dried pure alginate scaffold, and alginate/HNT composite scaffolds.

2.4.2. Mechanical property determinations

Compression testing of the scaffolds was carried out using the Zwick/Roell Z005 machine under 25 °C according to ASTM D5024-95a. The samples for the test were cylinder samples with a diameter of 10 mm and thickness of 10 mm. The crosshead speed was 2 mm/min, and up to failure or until 60% reduction in specimen height. The stress–strain curves for every sample were recorded automatically. The compressive properties of the scaffolds in wet state were tested by soaking the scaffolds in PBS solution at 37 °C for 24 h. At least five samples were used to obtain reliable data.

2.4.3. Scanning electron microscopy (SEM)

Before SEM observation, the scaffolds were sectioned and coated with 10 nm thick gold–palladium using a sputter coater (BALTEC SCD 005). The morphology of the scaffolds was observed with a Hitachi S-4800 FE–SEM at 2 kV.

2.4.4. Stereoscopic microscope

The three-dimensional structure of the scaffolds was studied using ZEISS SteREO Discovery. V20, Germany. The images were obtained at the surface and at different depths approaching ~1000 μm along the z-axis.

2.4.5. Thermogravimetric analysis (TGA)

TGA of the scaffold was carried out with NETZSCH TG 209F3 Tarsus® from room temperature to 600 °C at a heating rate of 10 °C/min under N_2 atmosphere.

2.4.6. X-ray diffraction (XRD)

XRD profiles for samples were obtained using X-ray diffractometer (D8, Bruker Corporation) at room temperature. The CuKa radiation source was operated at 40 kV power and 40 mA current. The scanning angle was from 5° to 50°.

2.4.7. Porosity measurement

The porosity of the scaffolds was determined using the reported method [19]. First, the scaffolds were immersed in absolute ethanol until it was saturated. Afterwards, the scaffolds were weighed before and after the immersion in alcohol. The porosity was calculated using the formula,

$$\text{porosity} = \frac{W_2 - W_1}{\rho V_1} \times 100\%.$$

Here, W_1 and W_2 were the weight of scaffold before and after immersion in alcohol, respectively. V_1 is the volume before immersion in alcohol; and ρ is a constant (the density of alcohol). All samples were triplicated in the experiment. Three parallel sets were analyzed for every scaffold and the mean value of the porosities of different scaffolds was taken.

2.4.8. Water uptake abilities

The water uptake ability (E_A) of scaffold was studied using the following procedure. Dry scaffolds were weighed (W_{dry}) and immersed in distilled water for 48 h. Then the scaffolds were gently removed from the beaker after 48 h and placed on a wire mesh rack. Excessive water was drained and scaffolds were weighed (W_{wet}) to determine water uptake. Three parallel sets were analyzed for every scaffold and the mean value was taken.

$$E_A = \frac{W_{wet} - W_{dry}}{W_{dry}} \times 100\%$$

2.4.9. In vitro biodegradation behavior

The scaffolds were equally weighed and immersed in lysozyme (10,000 U/mL) containing the PBS medium and incubated at 37 °C.

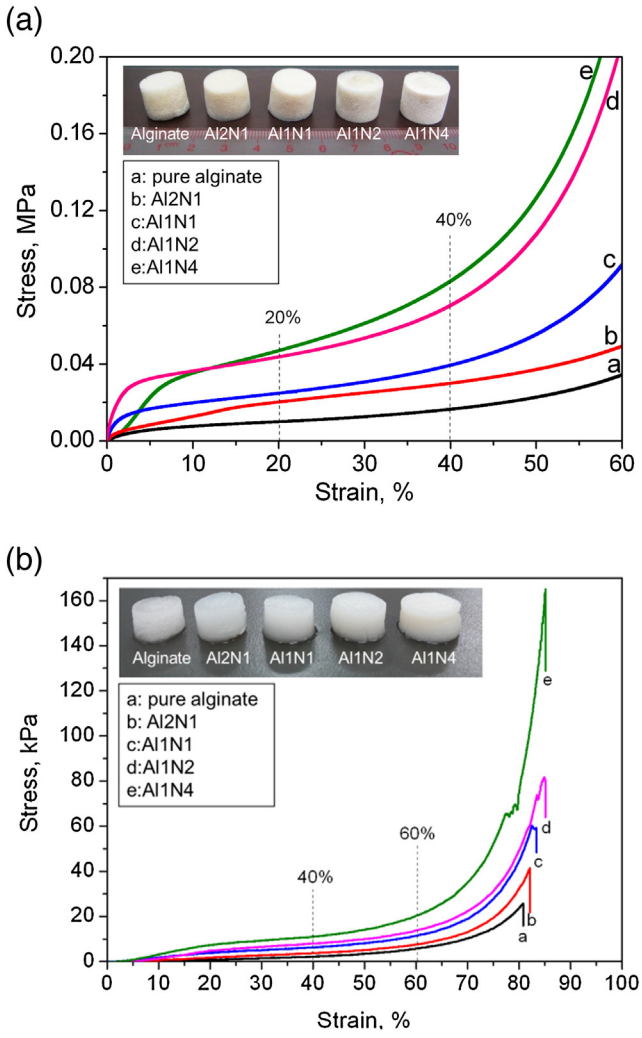

Fig. 4. Compressive stress–strain curves of alginate and alginate/HNT composite scaffolds in dry (a) and wet (b) states. The inset is the appearance of the alginate/HNT composite scaffolds in dry and wet states.

The samples were removed after 7, 14, 21 and 28 days and washed with deionized water to remove ions adsorbed on surface and freeze-dried. The dry weight was noted as W_t and initial weight as W_i. The degradation ratio of the scaffolds was calculated using the following formula. Three parallel sets were analyzed for every scaffold and the mean value was taken.

$$\text{degradation ratio} = \frac{W_i - W_t}{W_i} \times 100\%$$

Table 1
Summary of the mechanical properties of the alginate–HNT composite scaffolds in dry and wet state (data obtained from Fig. 4).

Sample	Stress at 20% strain in dry state (kPa)	Stress at 40% strain in dry state (kPa)	Elastic modulus in wet state (kPa)	Stress at 40% strain in wet state (kPa)	Stress at 60% strain in wet state (kPa)
Alginate	10.0	16.3	8.41	2.2	5.7
Al2N1	20.2	30.1	10.9	3.7	7.5
Al1N1	24.7	39.3	15.9	6.3	11.4
Al1N2	43.7	70.4	25.4	8.0	13.8
Al1N4	47.0	83.0	43.7	11.0	20.2

2.4.10. Cell adhesion and growth on pure alginate and alginate/HNT composites

BALB/c-3T3 mouse fibroblast cells were cultured in Dulbecco's modified Eagle's medium (DMEM) supplemented with 10% fetal bovine serum (FBS) and 1% antibiotic in an incubator with 5.0% CO_2 at 37 °C. The medium was changed every 3 days. Cells were routinely removed from tissue culture polystyrene (TCPS) dish with 0.25% trypsin–EDTA and plated on different substrates.

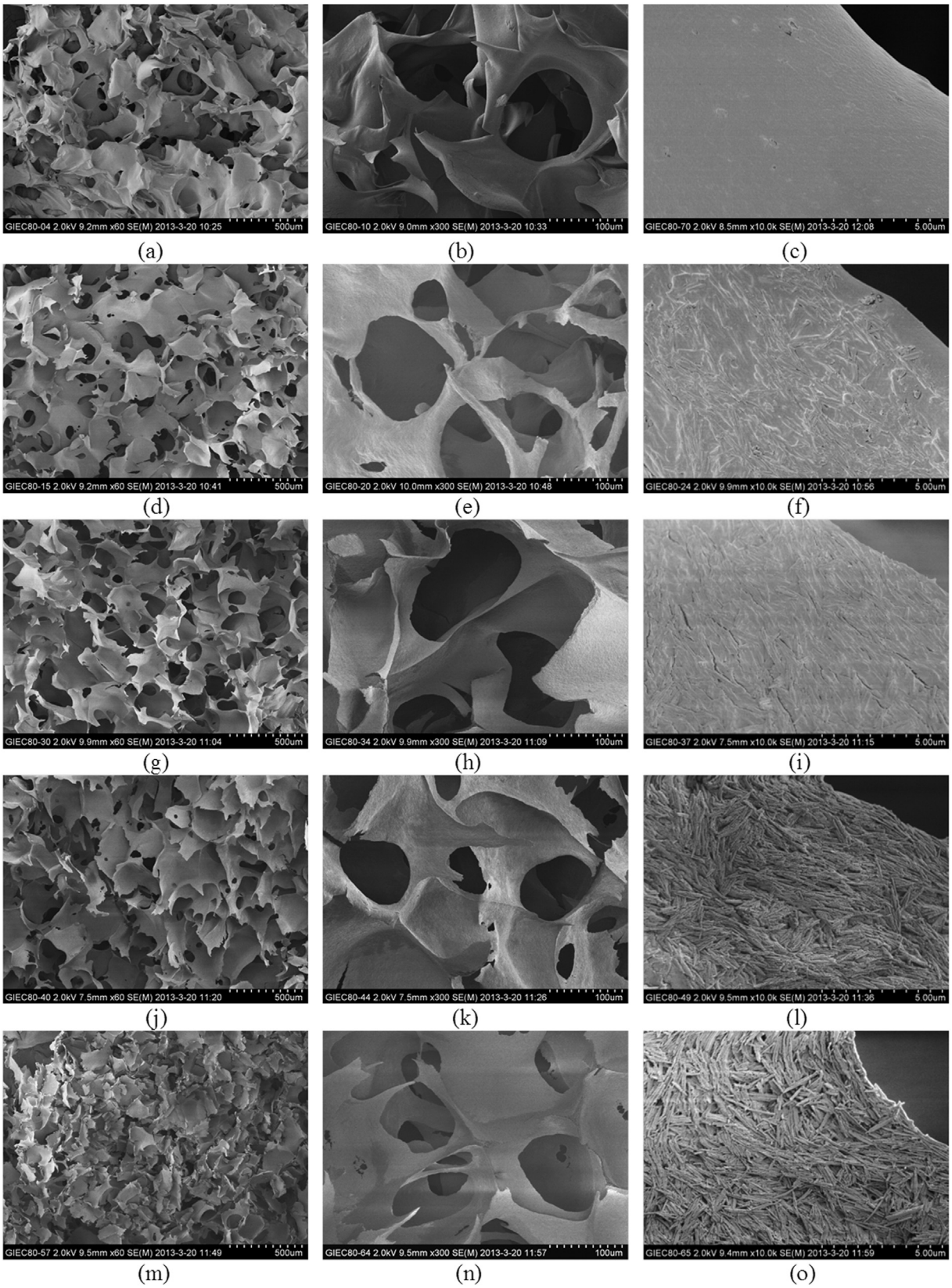

Fig. 5. SEM photos of freeze-dried pure alginate and alginate/HNT composite scaffolds with different magnifications: pure alginate (a–c); Al2N1 (d–f); Al1N1 (g–i); Al1N2 (j–l); Al1N4 (m–o).

The seeding cell density of 96 well culture plates was 2.0×10^4 cell/mL.

The cytocompatibility of the alginate–HNT composite was firstly assessed by the attached cell morphology and numbers on the corresponding films. All films remained transparent even with high HNTs loadings, which allowed the direct observation of cell morphology by an inverted phase contrast microscope. For assessing cell morphology, the random images of cells on each substratum

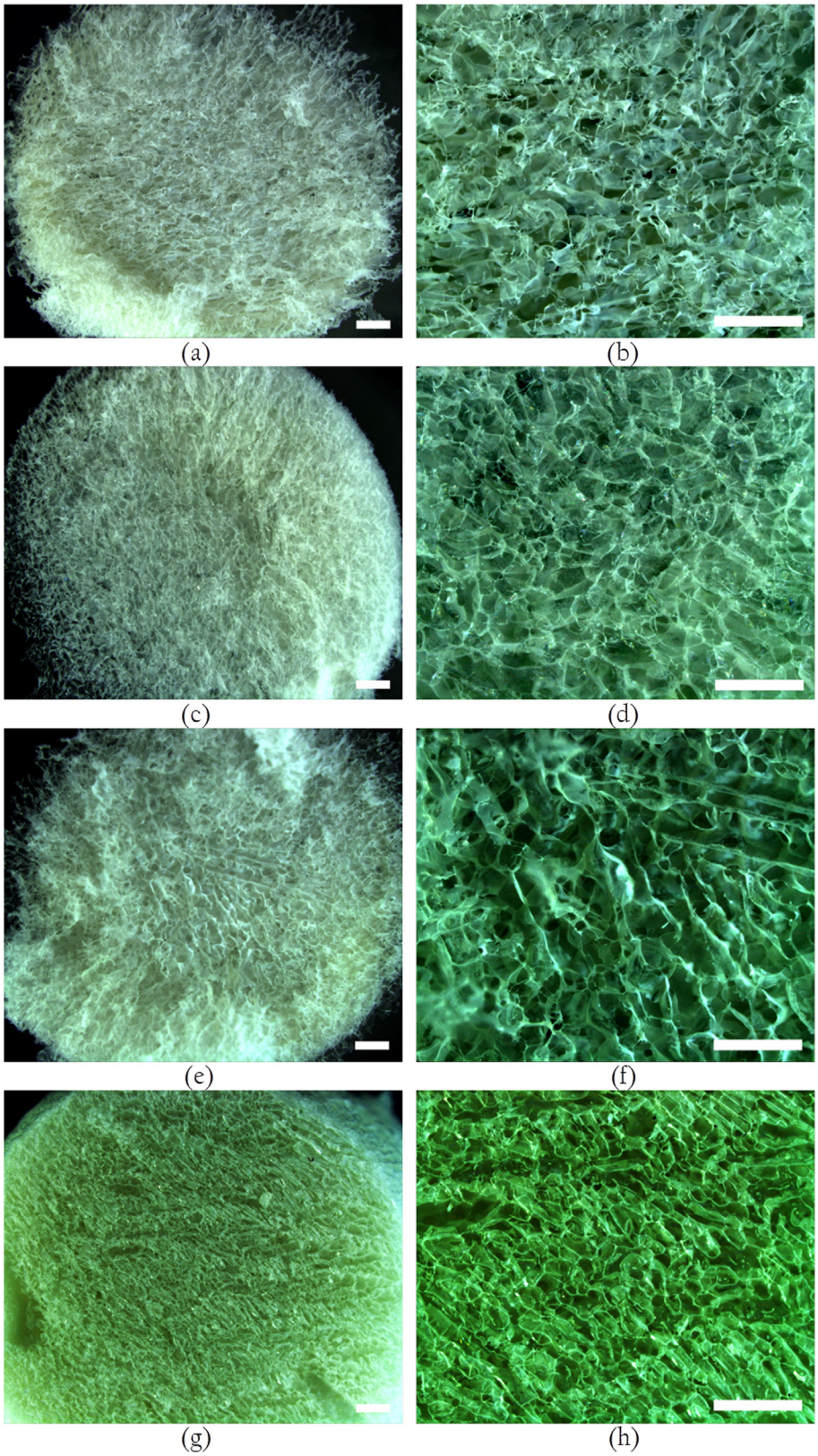

Fig. 6. Stereoscopic microscope micrographs of the pure alginate and alginate/HNT composite scaffolds: (a, b) pure alginate; (c, d) Al2N1; (e, f) Al1N1; (g, h) Al1N2; (i, j) Al1N4. The scale bar in the photos represents 1000 μm.

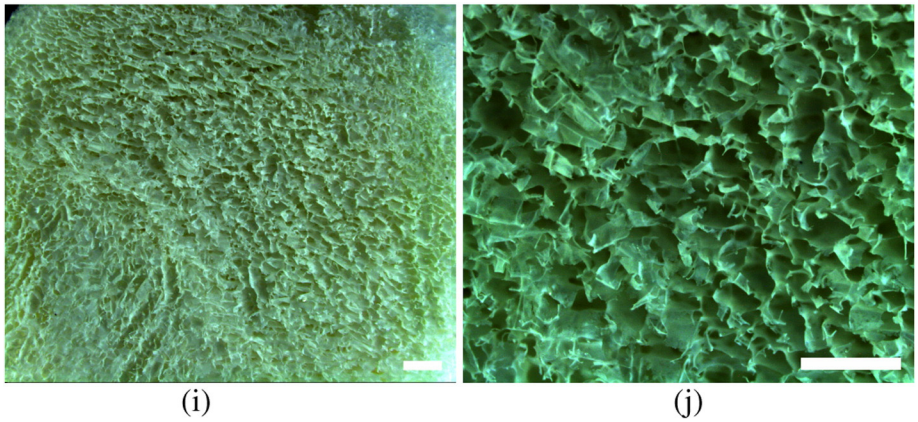

Fig. 6 (*continued*).

were acquired using a CCD camera after culturing 1 day in regular media.

After 3 days of culture on the pure alginate and alginate/HNT composite films, cells were rinsed carefully with a warm phosphate buffer solution (PBS) to remove non-adherent cells. All samples were fixed with 4% paraformaldehyde in PBS for 30 min and then permeabilized with a 0.1% v/v Triton X-100 for 5 min. For fluorescence staining, the cells were incubated with 1 mg/mL Phalloidin-TRITC (Sigma) for 1 h at room temperature to label the filamentous actins. After thoroughly rinsed, nuclei were stained with 5 mg/mL 4′,6-diamidino-2-phenylindole (DAPI, Sigma) for 15 min. All the stained samples were rinsed extensively with PBS, prior to observation under an immunofluorescence microscope (IX71, Olympus) mounted with CCD.

SEM analyses were performed to observe the morphology of the cells grown on the pure alginate and alginate/HNT composite scaffolds. At the third day, the medium was removed and the samples were washed twice with PBS. The cells were then fixed with 2.5% glutaraldehyde in cacodylate buffer (Karnovsky fixation solution) for 24 h at 4 °C. Then, the specimens were washed with cacodylate buffer several times and the dehydration of the cells attached to the films was done in ethanol at 30, 50, 70, 80, 90, 95 and 100%. Then the samples were freeze-dried at −80 °C. The morphologies of the cells attached to the alginate and alginate/HNT composite scaffolds were observed by a Philips XL30 ESEM machine.

Cell proliferation on the pure alginate and alginate/HNT composite scaffolds was assessed by dimethylthiazol diphenyl tetrazolium bromide (MTT) assay. Ca^{2+} cross-linked scaffolds were seeded with the cells in DMEM cell culture medium with a density of 1×10^5 cells/well in 24-well cell culture plates. The plates were incubated at 37 °C in a 5% CO_2 incubator. At the time point of 1, 4, and 7 days, the absorbance of the extracted dye, which is proportional to the number of cells attached to the scaffold, was measured spectrophotometrically with a microplate reader (Bio-Rad, Model 680, USA) at wavelengths of 570 nm. Experiments were run in triplicate per sample. All data were expressed as the mean ± standard deviation (SD) for n = 3.

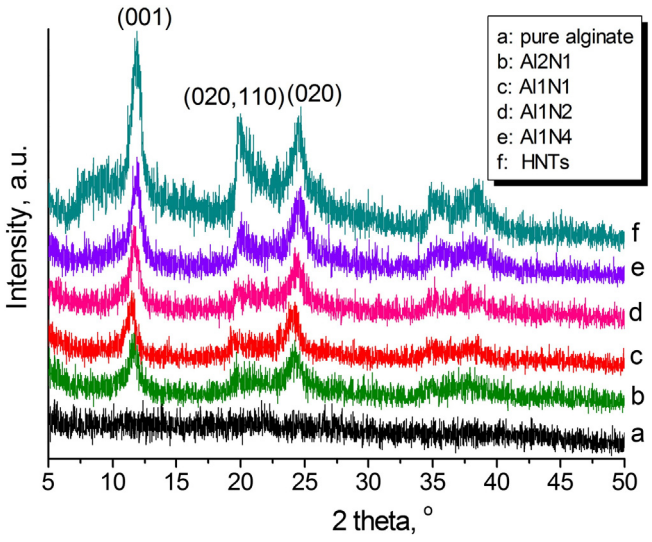

Fig. 7. XRD patterns for alginate, HNTs and alginate/HNT composite scaffolds: (a) pure alginate; (b) Al2N1; (c) Al1N1; (d) Al1N2; (e) Al1N4; (f) HNTs.

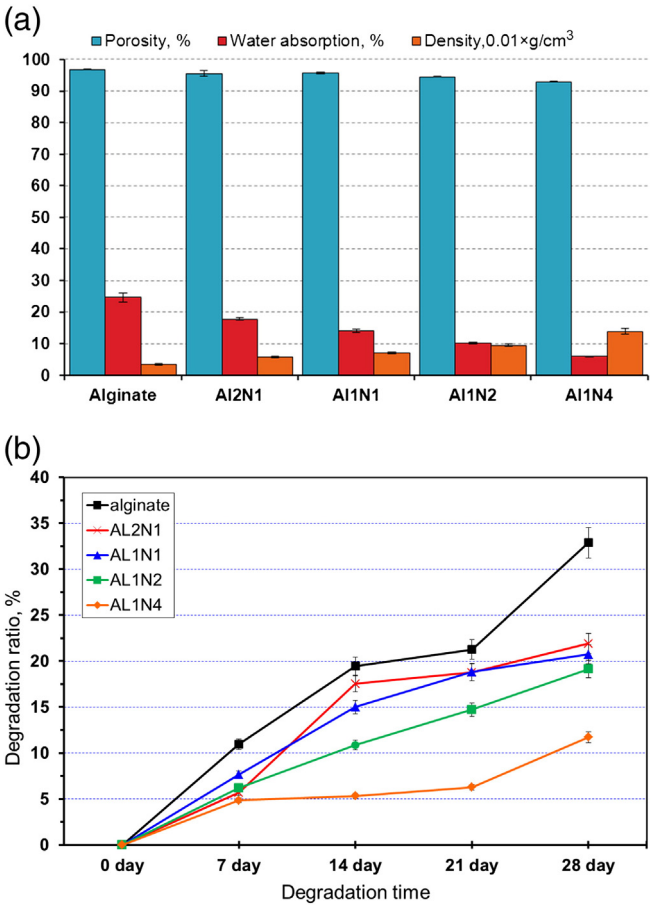

Fig. 8. Density, porosity, water absorption (a), and degradation behavior in PBS solution (b) of freeze-dried alginate and alginate/HNT composite scaffolds.

3. Results and discussion

3.1. The interactions between alginate and HNTs

Morphology analysis was carried out to elucidate the interactions between the alginate and HNTs. The structure and morphology of the pristine HNTs and alginate–HNTs were firstly evaluated by AFM measurements (Fig. 1). The AFM images of the pristine HNTs show that their surface is relatively smooth, sharp, and distinguishable. In the case of the alginate–HNTs, it can be seen that the walls of the tubes are rough and indistinct possibly due to the wrapping the alginate chains. From the height profile as shown in Fig. 1(e, f), the overall diameters of the alginate–HNTs increase due to the wrapping of alginate (from a maximum of about 85 nm of pristine HNTs to 115 nm for the alginate–HNTs). TEM was further used to character the wrapping of the alginate on the HNTs (Fig. 2). The high resolution TEM images were taken for the pristine HNTs and the alginate–HNTs (weight ratio, 2:1). The thicker tube walls and partially filling of the inner tube space are found for the alginate–HNT samples (Fig. 2b). An organic layer with light gray color in several nanometers is located on the surfaces of the tubes (Fig. 2d). This indicates that the alginate polymer layers exist on both the inner and outer surfaces of HNTs due to their interactions. For the TEM photos of pristine HNTs, clear and smooth external surfaces are observed. The wrapping of polymer layer around nanotubes via covalent bond [20] or physical interactions [13] has also been found in other polymer–nanotube hybrid systems [21,22]. The morphology results give the direct evidence of the polymer being coated on the surface of HNTs due to the interfacial interactions between alginate and HNTs which is a benefit for the preparation of high performance nanocomposites.

The zeta potentials of the dilute HNTs and alginate–HNT (2:1, weight ratio) aqueous dispersion (0.05 wt.%) have been determined. The HNTs dispersions have a zeta potential value of -30.7 ± 1.5 mV due to the negatively charged character which is related to the silica groups located on their outer surfaces [23]. The alginate–HNT dispersions exhibit a zeta potential of -65.8 ± 0.5 mV. The decreased value is due to the negatively charged alginate polymer. FTIR analysis was also carried out to elucidate the interactions between the alginate and HNTs. The FTIR spectra obtained for pristine HNTs, pure alginate and alginate/HNT composite are presented in Fig. 3. The spectra of pure alginate and pristine HNTs are consistent with those reported in the literature [24,25]. Alginate displays adsorption bands at 3365 cm^{-1}, 1628 cm^{-1} and 1419 cm^{-1} which correspond to OH stretching, asymmetric $-COO^-$ stretching vibration (ionic crosslinked) and symmetric $-COO^-$ stretching vibration, respectively. Pristine HNTs show the adsorption bands at 3695 cm^{-1}, 1032 cm^{-1} and 911 cm^{-1} which correspond respectively to O–H stretching of inner-surface hydroxyl groups, Si–O stretching and Al–O bending [25]. The FTIR spectra of the composites show the combined peaks of alginate and HNTs (except the overlapping of the peaks), indicating the successful incorporation of HNTs into the alginate scaffold. However, the transmission bands at 3365 cm^{-1} of alginate and 3695 cm^{-1} of HNTs are slightly shifted in the composites, indicating the possible hydrogen bonding interactions between their hydroxyl groups. Also, the peak around 1419 cm^{-1} of alginate, which corresponds to the symmetric $-COO^-$ stretching vibration, shifts to higher wavenumber in the composites. However, neither noticeable variations in the position of the FTIR peaks nor the appearance of new peaks by the incorporation of other nanoparticles into alginate was found [6]. Therefore, from the present FTIR results a physical interaction mainly the hydrogen bonds occur between HNTs and alginate, which is a benefit for the performance improvement of the composite scaffolds.

3.2. Mechanical properties of the alginate/HNT composite scaffolds

Based on the interactions between alginate and HNTs, alginate/HNT composite scaffolds were prepared by solution-mixing and freeze-drying technique. The appearance of the prepared scaffolds is shown in Fig. 4(a) inset. It can be seen that all the scaffolds show a uniform shape in the form of sponge. HNTs have little influence on the color, shape, and porosity of the alginate scaffolds. But by touching them by hand, an obvious stiffening of the composite scaffolds is found compared with the mechanically weak pure alginate scaffolds. The compressive stress–strain curves of alginate scaffolds with and without HNTs are shown in Fig. 4(a). The summarized mechanical property data is listed in Table 1. It can be seen that the composite scaffolds are generally stronger and more robust than the pure alginate scaffolds. The stress at the same strain of the composite scaffolds is far above that of the pure alginate scaffolds. For example, the compressive strength of the Al1N4 at 20% and 40% strain increases by factors of 3.74 and 4.06 respectively in comparison to pure alginate scaffold. From the initial stage of the stress–stain curves, the slope of the composite scaffolds is higher than that of pure alginate sample. This suggests the increased compressive modulus of the composite scaffolds compared to the pure alginate scaffold. The high reinforcing ability of HNTs on the alginate can be attributed to their capability of effectively enduring and transferring the stress via the composite interfaces. The changed density and porosity of the alginate scaffold by the addition of HNTs can also affect on the mechanical properties which will be shown in the following sections. In our previous study, HNTs have a similar reinforcing ability for porous chitosan scaffolds used in tissue engineering materials [13].

It is important to determine the mechanical properties of the scaffolds in wet state, since the scaffolds need to contact the body fluid when they are implanted in the body. The compressive properties of

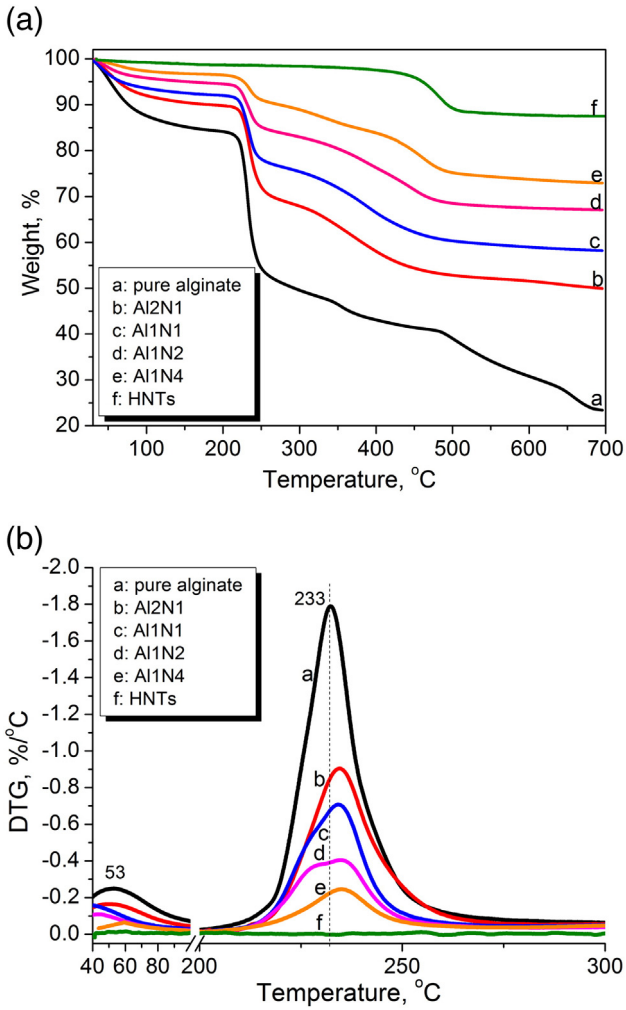

Fig. 9. TG (a) and DTG (b) curves for alginate, HNTs and alginate/HNT composite scaffolds.

the scaffolds in wet state were tested by soaking the scaffolds in PBS solution at 37 °C for 24 h. The typical stress–strain curve for the sample in wet state is shown in Fig. 4(b). The mechanical properties for both the pure alginate and the composite scaffolds are dramatically decreased when the scaffolds are wetted by PBS solution. It can be seen that HNTs can also effectively reinforce the alginate scaffold in wet state. The elastic modulus, the stress at 40% strain, and the stress at 60% strain of the alginate scaffold significantly increase after the incorporation of the HNTs. For example, the Al1N4's elastic modulus, the stress at 40% strain, and the stress at 60% strain are 43.7 kPa, 11.0 kPa, and 20.2 kPa, which are 4.2, 4.0, and 2.5 folds than those of the pure alginate scaffold respectively. Therefore, the alginate/HNT composite scaffolds can tolerate much higher loading both in dry state and wet state. Since the tissue engineering scaffolds should act as temporary physical support to withstand the stresses until the tissues are regenerated, the improved strength is a benefit for their practical applications.

3.3. Microstructures of the alginate/HNT composite scaffolds

The pore size of scaffolds affects cell adhesion, proliferation, and differentiation. The scaffold pore size must be small enough to ensure mechanical integrity, but large enough to cell growth and the nutrient diffusion needs of the tissue [26]. The cross-section morphologies of the scaffold observed by scanning electron microscopy (SEM) are shown in Fig. 5. The pure alginate scaffold exhibits a highly porous structure with interconnected pores with size in the range of 100–200 μm (Fig. 5b), which is in accordance with other reports [6,27]. When HNTs are introduced into alginate with different loadings, the composite scaffolds also show a regular network structure with numerous pores even when the loading is as high as 80 wt.%. Nearly no differences from the SEM morphology can be identified among the samples, indicating that HNTs have little effects on the formation of ice crystal during the scaffold preparation. In the higher magnification images,

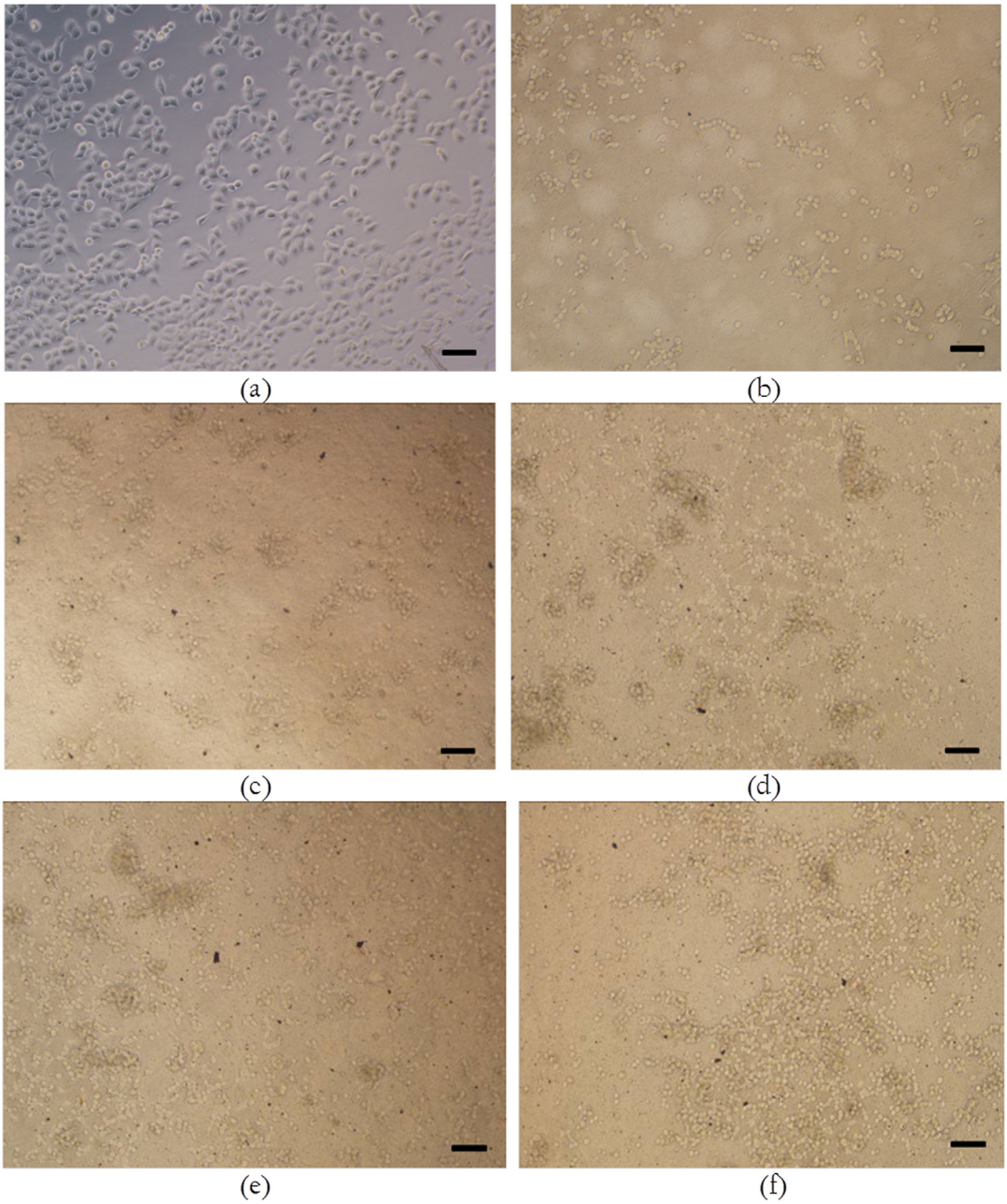

Fig. 10. Cell phase contrast micrographs at 24 h on TCPS (a), pure alginate (b), Al2N1 (c), Al1N1 (d), Al1N2 (e) and Al1N4 (f) films. The black bars in the photos represent 100 μm.

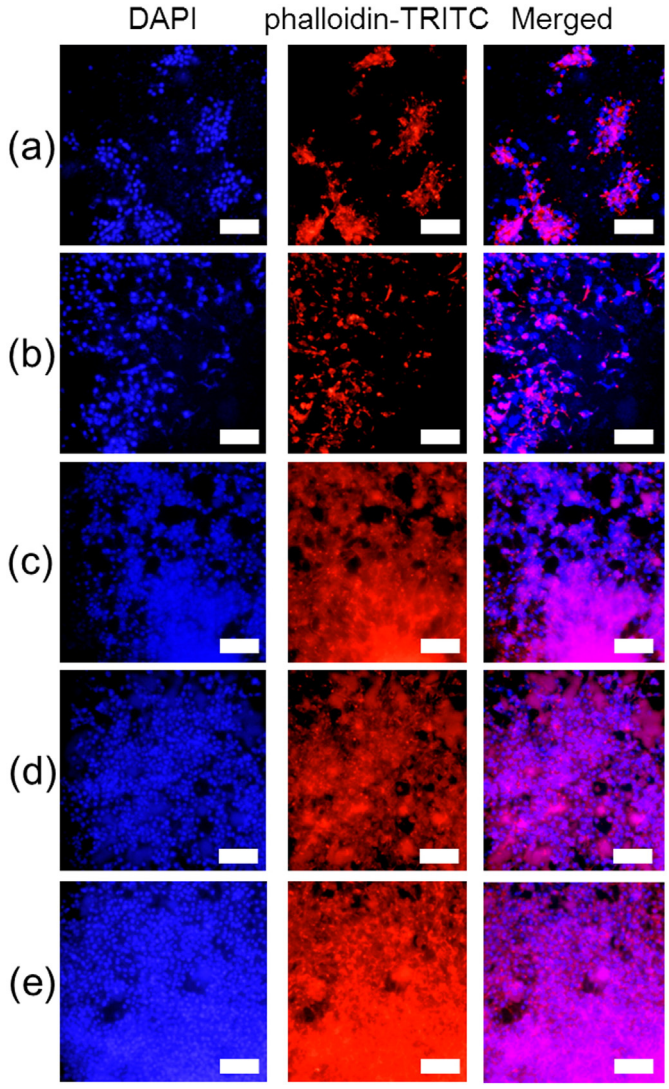

Fig. 11. Fluorescent micrographs of NIH3T3 cells on pure alginate and alginate–HNT composite scaffolds after 3 days of culture: (a) alginate; (b) Al1N2; (c) Al1N1; (d) Al1N2; (e) Al1N4. The cells were stained to label the nuclei (DAPI, left column) and filamentous actins (phalloidin–TRITC, middle column). The last column shows the merged photo of the first two photos for the same sample. The scale bar represents 100 μm.

HNTs are well embedded in the alginate matrix with blurry interface morphology. There is no apparent self-aggregation or microphase separation of HNTs in the alginate matrix in spite of the high HNTs content, indicating the good interfacial bonding in the systems. In previous study, the addition of hydroxyapatite (HAP) to the polymer solution also did not change the morphology of the alginate scaffold [27].

To analyze the 3D architecture of the scaffolds, stereoscopic microscope analysis was performed. Micrographs (Fig. 6) of the scaffolds reveal a uniform porous structure at different angles and depths. Consistent with SEM results, all the alginate/HNT composite scaffolds are highly porous and interconnected with a pore size of around 100–200 μm. The pore shape and dimension of the composite scaffolds (Fig. 6(c) to (j)) are similar to the pure alginate scaffolds (Fig. 6(a) and (b)). However, the strength of the pore walls increases with increasing HNTs content while the pore walls of the pure alginate scaffold collapse and appear to be agglomerated. This also supports the reinforcing effect of the nanotubes to the soft polymer matrix as illustrated as the compressive property determination.

The XRD patterns of the scaffolds are shown in Fig. 7. Pure alginate shows no obvious peak due to its amorphous state. By incorporation of HNTs, the composite shows the diffraction peaks around $2\theta = 11.9°$, 20°, and 25° which are assigned to (001), (020,110), and (020) plane of HNTs respectively [28]. The peak around 12° of HNTs in the composite scaffolds increases with the loading of HNTs, indicating the homogeneous mixing of alginate and HNTs. The location of the diffraction peaks of HNTs in the composite scaffolds remains unchanged, suggesting that no intercalation of alginate into the interlayer of tube occurs. Interestingly, the intensity of the peak corresponding to the (020,110) plane decreases with the increase of HNTs loading, which has also been found in other polymer–HNT composite systems [13,29]. The possible explanation for this phenomenon is that a partial orientation of HNTs takes place within the alginate matrix via the interfacial interactions. From the XRD result, HNTs can be uniformly distributed and partly oriented in the composite scaffolds but their layer space remains unchanged.

3.4. Physico-chemical properties of the alginate/HNT composite scaffolds

Fig. 8 compares the density, porosity, and water uptake of the prepared alginate and alginate/HNT composite scaffolds. The density of the sample ranges from 0.035 to 0.139 g/cm^3. Pure alginate scaffold exhibits the lowest density among the samples. By addition of HNTs, the density of the composite scaffolds linearly increases with HNTs concentration. The increased density of composite scaffolds is due to the greater material content in the same scaffold volume, since we fix the water volume during the preparation of the scaffolds. The increased density of the scaffold contributes to the improvement of compressive performance for the composite scaffolds. In addition, scaffold porosity is essential in intestinal tissue engineering in order to facilitate cell migration and nutrient transport. All the scaffolds show high porosity in the range of 93–97%, which satisfies the requirement for applications in tissue engineering. The porosity of samples is slightly decreased by the incorporation of HNTs, which is also attributed to the higher material content in the composite scaffolds. Previous report showed that the incorporation of HAP into chitosan led to slightly decreased porosity of the scaffold [30].

Water uptake of scaffolds is also important for tissue engineering scaffold because the absorption of physiological fluid and metabolites occurs through the scaffolds. Pure alginate scaffold has a water absorption of 24.6% which is higher when compared to alginate/HNT composite scaffolds. The addition of HNTs to alginate leads to a decrease in the degree of water absorption. This result can be attributed to the decrease in the polymer ratio in the composite scaffold. Since the water absorption of the nanoclay is limited, it is considered that the water absorption of the scaffold is mainly attributed to the polymer networks. As a consequence, the decreased polymer content in the composite scaffold results in a decreased water uptake ratio. In addition, the HNTs can act as physical crosslinking points for alginate due to the hydrogen bond interactions, which results in the increased entanglement of the alginate and limited the mobility of the polymer chains [9]. This also leads to the decreased water absorption of the composite scaffolds. As evident from these results, the density, porosity and water absorption of alginate/HNT composite scaffolds are composition dependent and can be tailored according to the practical applications in tissue engineering.

The degradation behaviors of the pure alginate and alginate/HNT composite sponges were monitored as a measure of weight loss in biological buffer (PBS) over 28 days (Fig. 8b). It can be seen that the degradation ratio of all the samples in the PBS increases with the increase in the soaking time. The pure alginate scaffolds lost about 33% of their weight after 28 days of incubation with lysozyme. Compared with pure alginate scaffold, the composite sponges show decreased weight loss ratio. This is attributed to the primary degradation of the sample that is related to the polymer chain breakage while HNTs nearly do not degrade in PBS solutions. With the increase of the HNTs loading, the relative contents of the alginate in the composite decrease. Therefore, the weight loss ratio of the composites decreases with the increase

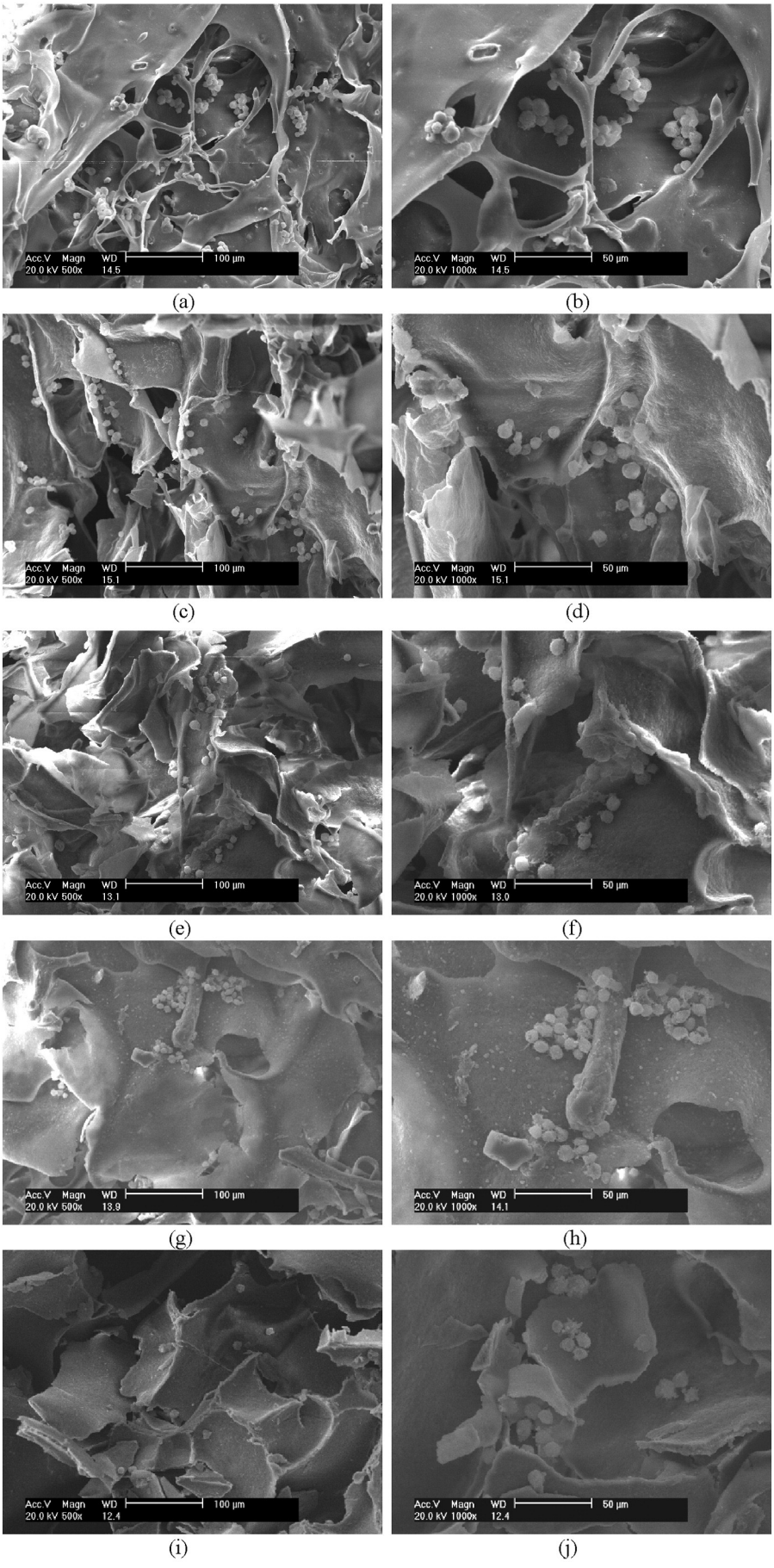
Acc.V Magn WD 100 μm
20.0 kV 500x 14.5
(a)
Acc.V Magn WD 50 μm
20.0 kV 1000x 14.5
(b)
Acc.V Magn WD 100 μm
20.0 kV 500x 15.1
(c)
Acc.V Magn WD 50 μm
20.0 kV 1000x 15.1
(d)
Acc.V Magn WD 100 μm
20.0 kV 500x 13.1
(e)
Acc.V Magn WD 50 μm
20.0 kV 1000x 13.0
(f)
Acc.V Magn WD 100 μm
20.0 kV 500x 13.9
(g)
Acc.V Magn WD 50 μm
20.0 kV 1000x 14.1
(h)
Acc.V Magn WD 100 μm
20.0 kV 500x 12.4
(i)
Acc.V Magn WD 50 μm
20.0 kV 1000x 12.4
(j)

of HNTs content. The interfacial interactions between HNTs and alginate can lead to physical crosslinking network in the composites, which also can protect the alginate against the attack of the enzyme. The decreased degradation rate of biopolymers by addition of nanoparticles can increase the stability against enzymatic degradation, which has also been reported in other alginate composite systems [6,31].

3.5. Thermal properties of the alginate/HNT composite scaffolds

Thermogravimetric analyses can supply information on the thermal stability of materials, which are widely used to study interfacial interactions in composites. TGA was conducted on pure alginate and alginate/HNT composite scaffold. The introduction of HNTs has an influence on the thermal stability of the alginate due to the interfacial interaction (Fig. 9). The TGA curves of both scaffolds exhibit the same trend: the weight of sample decreases gradually from room temperature to 220 °C; in the range of 220–270 °C the weight declines sharply and then decreases slightly from 270 to 500 °C. The weight loss below 220 °C can be ascribed to the loss of free water, bonded and decomposition of oligosaccharide, while the rapid weight loss upon 200 °C involves the complex process of degradation of polysaccharides. From the DTG curves (Fig. 9b), the maximum degradation temperature of alginate in the composite slightly shifts to higher temperature compared to the pure alginate. This can be explained that HNTs can improve the thermal stability of the alginate. The residual mass of the composite scaffold is higher than that of pure alginate scaffold over the whole test temperature range, which is attributed to the introduction of HNTs and the interfacial interactions. After 500 °C, the alginate scaffold losses the weight rapidly, which is due to the serious degradation at high temperature of the polymer chains.

3.6. Cell attachment of the alginate/HNT composite scaffolds

For tissue engineering application, the scaffolds are expected to promote cellular adhesion, proliferation, and differentiation. Cytocompatibility of the pure alginate and alginate/HNT composite scaffolds was assessed with fibroblast 3T3 cells. The cell attachment and proliferation of 3T3 cells on the materials were firstly studied using the phase contrast micrographs (Fig. 10). The morphology of these cells seeded on the alginate/HNT composites exhibit no obvious variances between different concentrations. Fibroblast cells display round or fusiform shape on the surfaces of both pure alginate and alginate/HNT composites at 24 h after seeding, indicating that the cells can attach on these material surfaces. The relative number of the attached cells on the alginate/HNT composites increases with the HNTs content. This may be attributed to the good cytocompatibility of HNTs which has also been confirmed in previous studies [13,14,23,32]. Also the increased surface roughness of the polymer by HNTs may promote the cell attachments [31]. DAPI stained nuclei and phalloidin–TRITC stained skeleton fluorescent images of these cells are shown in Fig. 11. The fluorescent images also show that the cell number increases in the composite compared with the pure alginate, suggesting the enhanced attachment and proliferation of cells on the composite by the incorporation of HNTs. Within 72 h of incubation, the cells of rounded morphology further flatten and spread evenly throughout the surface of the scaffolds. The enhanced attachment and proliferation are also due to the biocompatibility of HNTs and the increase in the surface roughness of the composites.

To further investigate the influence of HNTs on the cytocompatibility of alginate scaffold and the cell distribution on the 3D porous scaffolds, SEM images were taken after 3 days of culture (Fig. 12). It can be seen that cells are attached to both the scaffold surface and the inner pores of the scaffolds. The spherical cells are found on these scaffolds, suggesting that the cells are growing and proliferating after 3 days of incubation. In the case of composite scaffolds with relative low HNTs content (Al2N1, Al1N1), a homogeneous cell distribution is observed. In these scaffolds, the cells are predominantly attached to the inner pore surface, and only a few cells are attached to the outermost surface. While for the pure alginate scaffold and the composite scaffolds with high HNTs loadings (Al1N2, Al1N4), the cells tend to aggregate. This may be explained by the fact that the cells are confined to growth space either because of the improper pore structure or the improper chemical composition (high HNTs loadings). The uniform cell adhesion in the inner pores suggests that the identical medium flow through each repeating unit of the interconnected pores of the composite scaffolds. The incorporation of hydrophilic and biocompatible HNTs improves the interfacial adhesion with the cell membrane and promotes attachment and proliferation of cells. Hence, the cell culture experiment results demonstrate the alginate/HNT composite is biocompatible and has potential applications in tissue engineering.

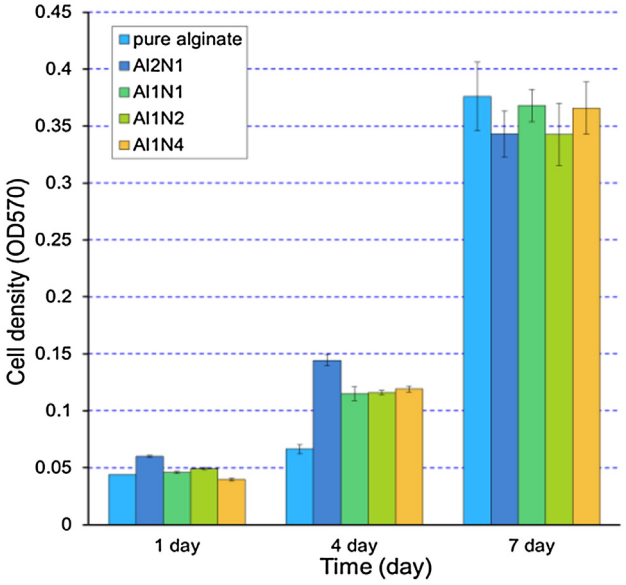

Fig. 13. Viability of fibroblast NIH3T3 cells on pure alginate scaffold and alginate/HNT composite scaffolds as a function of time, measured by MTT assay which represents active mitochondrial activity of living cells.

The biocompatibility of the scaffolds has been assessed by MTT method using NIH3T3 cells, and the results are summarized in Fig. 13. It can be seen that the cell growth increases continually with the culture time for all the groups. The cell population is higher on the composite scaffolds than on the pure alginate scaffolds after 1, and 4 days of culture, especially for the composite scaffolds with relatively low HNTs content. For example, the cell viability determined by the absorbance at 570 nm of the Al2N1 composite scaffold is above 2-fold compared to the pure alginate scaffold. The increased cell viability also suggests the good cytocompatibility of the alginate/HNT composites. The addition of HNTs can promote the cell attachment, spreading and growth on the alginate scaffolds. The improved cell attachment is related the composite scaffolds with a relatively rough surface and increased adsorption of fibronectin [33]. However, the cell viability difference among the scaffolds becomes less after 7 days of culture, since all the groups show comparable cell density values. This is due to the limited cell growth space after 7 days of culture for all the scaffolds. In total, the cell viability test results also support the improved cytocompatibility of

Fig. 12. SEM of the cartilage cells on pure alginate and alginate–HNT composite scaffolds after 3 days of culture: (a) and (b) alginate; (c) and (d) Al1N2; (e) and (f) Al1N1; (g) and (h) Al1N2; (i) and (j) Al1N4.

the alginate scaffolds by the incorporation of HNTs. Thus, alginate/HNT composite is a promising material for tissue engineering.

4. Conclusions

Alginate/HNT composite scaffolds were prepared by solution-mixing and freeze-drying technique. A layer of alginate is found on the outer surface of HNTs. The hydrogen bond interactions between HNTs and alginate are confirmed by FTIR result. The compressive stress both in dry and wet states at the same strain of the composite scaffolds is far above that of the pure alginate scaffolds. HNTs are well embedded in the alginate matrix with blurry interface morphology. HNTs can be uniformly distributed and partly oriented in the composite scaffolds but their layer space remains unchanged. All the scaffolds show high porosity in the range of 93–97% with pore size of around 100–200 μm, while HNTs have little effect on the pore structure. The addition of HNTs to alginate leads to a decrease in the degree of water absorption and degradation rate of the scaffold. HNTs can improve the thermal stability of the alginate. The relative number of the attached cells on the alginate/HNT composites increases with the HNTs content. The enhanced attachment and proliferation are attributed to the biocompatibility of HNTs and the increase in the surface roughness due to the incorporation of HNTs. Alginate/HNT composite scaffolds exhibit great potential for their application in tissue engineering.

Acknowledgments

This work was financially supported by the National Natural Science Foundation of China (grant No. 51473069), and the Guangdong Natural Science Funds for Distinguished Young Scholar (grant No. S2013050014606).

References

[1] J.A. Rowley, G. Madlambayan, D.J. Mooney, Alginate hydrogels as synthetic extracellular matrix materials, Biomaterials 20 (1999) 45–53.
[2] H.H. Tonnesen, J. Karlsen, Alginate in drug delivery systems, Drug Dev. Ind. Pharm. 28 (2002) 621–630.
[3] T. Joki, M. Machluf, A. Atala, et al., Continuous release of endostatin from microencapsulated engineered cells for tumor therapy, Nat. Biotechnol. 19 (2001) 35–39.
[4] L. Fan, J. Zhang, A. Wang, In situ generation of sodium alginate/hydroxyapatite/halloysite nanotubes nanocomposite hydrogel beads as drug-controlled release matrices, J. Mater. Chem. B 1 (2013) 6261–6270.
[5] C.K. Kuo, P.X. Ma, Ionically crosslinked alginate hydrogels as scaffolds for tissue engineering: part 1. Structure, gelation rate and mechanical properties, Biomaterials 22 (2001) 511–521.
[6] S. Srinivasan, R. Jayasree, K.P. Chennazhi, S.V. Nair, R. Jayakumar, Biocompatible alginate/nano bioactive glass ceramic composite scaffolds for periodontal tissue regeneration, Carbohydr. Polym. 87 (2012) 274–283.
[7] E.D. Yildirim, X. Yin, K. Nair, W. Sun, Fabrication, characterization, and biocompatibility of single-walled carbon nanotube-reinforced alginate composite scaffolds manufactured using freeform fabrication technique, J. Biomed. Mater. Res. B Appl. Biomater. 87B (2008) 406–414.
[8] A.D. Augst, H.J. Kong, D.J. Mooney, Alginate hydrogels as biomaterials, Macromol. Biosci. 6 (2006) 623–633.
[9] M. Kawaguchi, T. Fukushima, T. Hayakawa, et al., Preparation of carbon nanotube-alginate nanocomposite gel for tissue engineering, Dent. Mater. J. 25 (2006) 719–725.
[10] M. Liu, Z. Jia, D. Jia, C. Zhou, Recent advance in research on halloysite nanotubes—polymer nanocomposite, Prog. Polym. Sci. 39 (2014) 1498–1525.
[11] Y. Lvov, E. Abdullayev, Functional polymer–clay nanotube composites with sustained release of chemical agents, Prog. Polym. Sci. 38 (2013) 1690–1719.
[12] M. Liu, Y. Zhang, C. Wu, S. Xiong, C. Zhou, Chitosan/halloysite nanotubes bionanocomposites: structure, mechanical properties and biocompatibility, Int. J. Biol. Macromol. 51 (2012) 566–575.
[13] M. Liu, C. Wu, Y. Jiao, S. Xiong, C. Zhou, Chitosan–halloysite nanotubes nanocomposite scaffolds for tissue engineering, J. Mater. Chem. B 1 (2013) 2078–2089.
[14] M. Liu, Y. Shen, P. Ao, L. Dai, Z. Liu, C. Zhou, The improvement of hemostatic and wound healing property of chitosan by halloysite nanotubes, RSC Adv. 4 (2014) 23540–23553.
[15] L. Liu, Y. Wan, Y. Xie, R. Zhai, B. Zhang, J. Liu, The removal of dye from aqueous solution using alginate–halloysite nanotube beads, Chem. Eng. J. 187 (2012) 210–216.
[16] G. Cavallaro, A. Gianguzza, G. Lazzara, S. Milioto, D. Piazzese, Alginate gel beads filled with halloysite nanotubes, Appl. Clay Sci. 72 (2013) 132–137.
[17] Y. Wang, X. Zhang, Q. Wang, B. Zhang, J. Liu, Continuous fixed bed adsorption of Cu(II) by halloysite nanotube–alginate hybrid beads: an experimental and modelling study, Water Sci. Technol. 70 (2014) 192–199.
[18] S. Karnik, K. Hines, D.K. Mills, Nanoenhanced hydrogel system with sustained release capabilities, J. Biomed. Mater. Res. A (2014). http://dx.doi.org/10.1002/jbm.a.35376.
[19] Y. Zhang, M. Zhang, Synthesis and characterization of macroporous chitosan/calcium phosphate composite scaffolds for tissue engineering, J. Biomed. Mater. Res. 55 (2001) 304–312.
[20] S.K. Yadav, S.S. Mahapatra, M.K. Yadav, P.K. Dutta, Mechanically robust biocomposite films of chitosan grafted carbon nanotubes via the [2 + 1] cycloaddition of nitrenes, RSC Adv. 3 (2013) 23631–23637.
[21] J. Zhang, Z. Jia, D. Jia, D. Zhang, A. Zhang, Chemical functionalization for improving dispersion and interfacial bonding of halloysite nanotubes in epoxy nanocomposites, High Perform. Polym. (2015). http://dx.doi.org/10.1177/0954008314528226 (in press).
[22] C. Chao, J. Liu, J. Wang, et al., Surface modification of halloysite nanotubes with dopamine for enzyme immobilization, ACS Appl. Mater. Interfaces 5 (2013) 10559–10564.
[23] V. Vergaro, E. Abdullayev, Y.M. Lvov, et al., Cytocompatibility and uptake of halloysite clay nanotubes, Biomacromolecules 11 (2010) 820–826.
[24] G. Lawrie, I. Keen, B. Drew, et al., Interactions between alginate and chitosan biopolymers characterized using FTIR and XPS, Biomacromolecules 8 (2007) 2533–2541.
[25] P. Yuan, P.D. Southon, Z. Liu, et al., Functionalization of halloysite clay nanotubes by grafting with gama-aminopropyltriethoxysilane, J. Phys. Chem. C 112 (2008) 15742–15751.
[26] J.F.A. Valente, T.A.M. Valente, P. Alves, P. Ferreira, A. Silva, I.J. Correia, Alginate based scaffolds for bone tissue engineering, Mater. Sci. Eng. C 32 (2012) 2596–2603.
[27] H.-R. Lin, Y.-J. Yeh, Porous alginate/hydroxyapatite composite scaffolds for bone tissue engineering: preparation, characterization, and in vitro studies, J. Biomed. Mater. Res. B Appl. Biomater. 71B (2004) 52–65.
[28] G.W. Brindley, K. Robinson, D.M.C. MacEwan, The clay minerals halloysite and meta-halloysite, Nature 157 (1946) 225–226.
[29] M. Liu, Y. Zhang, C. Zhou, Nanocomposites of halloysite and polylactide, Appl. Clay Sci. 75–76 (2013) 52–59.
[30] J. Venkatesan, Z.-J. Qian, B. Ryu, N. Ashok Kumar, S.-K. Kim, Preparation and characterization of carbon nanotube-grafted-chitosan—natural hydroxyapatite composite for bone tissue engineering, Carbohydr. Polym. 83 (2011) 569–577.
[31] D. Depan, B. Girase, J.S. Shah, R.D.K. Misra, Structure–process–property relationship of the polar graphene oxide-mediated cellular response and stimulated growth of osteoblasts on hybrid chitosan network structure nanocomposite scaffolds, Acta Biomater. 7 (2011) 3432–3445.
[32] Y.-F. Shi, Z. Tian, Y. Zhang, H.-B. Shen, N.-Q. Jia, Functionalized halloysite nanotube-based carrier for intracellular delivery of antisense oligonucleotides, Nanoscale Res. Lett. 6 (2011) 1–7.
[33] W.W. Thein-Han, R.D.K. Misra, Biomimetic chitosan–nanohydroxyapatite composite scaffolds for bone tissue engineering, Acta Biomater. 5 (2009) 1182–1197.